Journal of Colloid and Interface Science 638 (2023) 363–374

Contents lists available at ScienceDirect

Journal of Colloid and Interface Science

journal homepage: www.elsevier.com/locate/jcis

# Nanostructured bio-based castor oil organogels for the cleaning of artworks

Giovanna Poggi [a], Harshal D. Santan [a], Johan Smets [b], David Chelazzi [a], Daria Noferini [c,d], Maria Laura Petruzzellis [e], Luciano Pensabene Buemi [e], Emiliano Fratini [a,*], Piero Baglioni [a,*]

[a] Department of Chemistry "Ugo Schiff" and CSGI, University of Florence, Via della Lastruccia 3, 50019 Sesto Fiorentino, (FI), Italy
[b] The Procter & Gamble Company, 1853 Strombeek-Bever, Brussels, Belgium
[c] European Spallation Source ERIC, 224 84 Lund, Skåne County, Sweden
[d] Jülich Centre for Neutron Science at Heinz Maier-Leibnitz Zentrum, Forschungszentrum Jülich GmbH, Lichtenbergstrasse 1, Garching, Garching
[e] Peggy Guggenheim Collection, Dorsoduro 701, 30123 Venice, Italy

## GRAPHICAL ABSTRACT

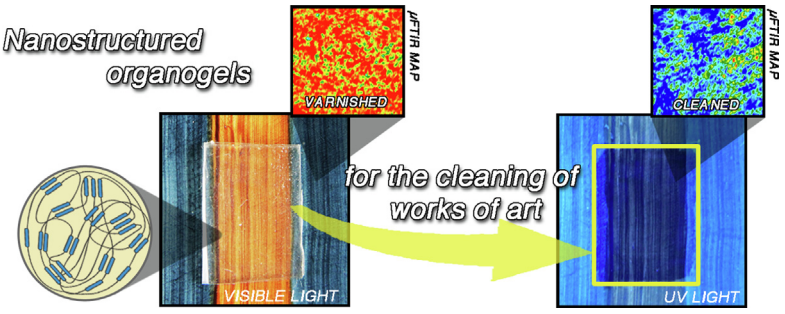


## ARTICLE INFO

*Article history:*
Received 28 November 2022
Revised 23 January 2023
Accepted 24 January 2023
Available online 1 February 2023

*Keywords:*
Organogels
Castor oil
Polyurethane networks
Cleaning
Cultural heritage conservation
Modern/contemporary art

## ABSTRACT

*Hypothesis:* Organic solvents are often used for cleaning highly water-sensitive artifacts in modern/contemporary art. Due to the toxicity of most solvents, confining systems must be formulated to use these fluids in a safe and controlled way. We propose here castor oil (CO) organogels, obtained thorough cost-effective sustainable polyurethane crosslinking. This methodology is complementary to previously demonstrated hydrogels, when conservators opt for organic solvents over aqueous formulations.
*Experiments:* The gels were characterized via Small-angle Neutron Scattering and rheology before and after swelling in two organic solvents commonly adopted in cleaning paintings. The removal of a photo-aged acrylic-ketonic varnish was evaluated under visible and ultraviolet light, and with FTIR 2D imaging.
*Findings:* The new gels are dry systems that can be easily stored and loaded with solvents before use. Their nanoscale organization, viscoelasticity and cleaning action are controlled changing the amount of crosslinking, the polymeric backbone, and the loaded solvents. The fluids are confined in the nanosized polymeric mesh of the gels, which are highly retentive, granting controlled release over delicate paint layers, and transparent, allowing monitoring of the cleaning process. These features, along with their sustainable synthesis, candidate the CO organogels as feasible solutions for cultural heritage preservation, expanding the palette of advanced tools for conservators over traditional thickeners.


* Corresponding authors.
*E-mail addresses:* emiliano.fratini@unifi.it (E. Fratini), baglioni@csgi.unifi.it (P. Baglioni).

https://doi.org/10.1016/j.jcis.2023.01.119
0021-9797/

## 1. Introduction

Cultural heritage assets have a fundamental role in the economic development of tourism and art industry [1] creating beneficial and inclusive social environments that improve citizens' life quality.[2–4] To maximize such benefits, the long-term conservation of irreplaceable artifacts and collections must be addressed. In this regard, science has been playing a crucial role in tackling the preservation of our artistic, historical and architectural heritage, providing methodologies and solutions that favor its transfer to future generations.[5] Nonetheless, while several diagnostic techniques have been developed over the last decades for investigating the composition and degradation of works of art,[6–8] there is still large room for the development of materials and methods to effectively counteract the degradation processes that inevitably affect works of art.[9–11] Recently, an additional requirement to all restoration materials is to cope with the fundamental requirements of the Green Deal, i.e. the tools and solutions adopted in art conservation must be safe to the environments and the operators, and based as much as possible on green chemistry. According to these principles, colloidal systems and soft matter with structural features in the micron-nano scale have proven to be essential tools to design innovative materials for remedial conservation, an approach that has led to dramatic enhancement of the effectiveness and durability of the restoration interventions.[5,9,12–18].

The removal of soil and unwanted materials from artifacts is a very common, delicate, and important task in the restoration of artworks. In particular, the cleaning of modern and contemporary works of art is highly challenging, as artists starting from the 1850s used materials derived from the industry, which typically display failure and instability,[19] mainly due to the presence of additives such as dryers, fillers and dispersion agents.[20] As a result, modern and contemporary paintings frequently exhibit pronounced sensitiveness to solvents and cleaning fluids.[21,22].

A fundamental strategy to deal with the cleaning of such highly delicate artifacts is the confinement of cleaning fluids and solvents in the micro and nanoporosity of gels, to selectively control their action and avoid damage to the original components of the artifacts. Traditionally, the conservation practice has mostly employed physical hydrogels or thickeners.[23] These are formed by intermolecular forces that poorly interconnect the gels' polymer chains, and therefore these systems are typically prone to leave gel residues on the surface of the artworks after standard cleaning procedures. In this regard, it has been shown that the complete removal of these residues is not achieved even after abundant rinsing with solvents, an invasive step that can cause leaching and swelling of the paint layers.[24,25] Besides, most traditional physical gels and thickeners have poor mechanical properties that hinder their feasible handling in restoration operations, and some of them, especially those based on polysaccharides, are susceptible to microbial attacks and temperature oscillations during storage.[26] To overcome these drawbacks, highly retentive hydrogel formulations with optimal mechanical properties have been recently developed for the safe and controlled cleaning of water-sensitive artworks,[27–33] expanding the palette of tools available to conservators. Recently, we showed by scattering and rheology measurements that uploading different complex aqueous fluids into chemical hydrogel networks induced changes in the nanostructure and viscoelastic properties of the gels, yielding formulations with optimal mechanical characteristics and retentiveness for cleaning artworks.[34] This approach can be useful to applicative fields even beyond cultural heritage conservation,[35–39] considering that the control of the nanostructure in 3D supramolecular gel networks remains a challenge.[40] However, options are still limited for interventions on artworks that cannot withstand the use of water, not even confined in a polymeric network. This is the case, for instance, of the removal of aged varnishes and protectives from modern and contemporary oil paintings and watercolors. It is worth noting that varnishes are usually sensitive to photoaging and oxidation, which results in discoloration and decreased solubility.[41–43] The selective and efficient removal of the varnish layer, without damaging the highly sensitive underlying paints, was deemed as risky with currently available state-of-the-art tools. We propose here a new class of castor oil organogels derived from natural resources using polyurethane crosslinking chemistry, tailored as a novel complementary tool to hydrogels for the cleaning of water-sensitive surfaces. Castor oil is of interest in the formulation of bio-based gel systems and soft matter with great applicative potential.[44,45] In this contribution, the overall synthetic route of the bio-based gels is sustainable and cost-effective, as it does not require any purification step. Differently from the few examples of organogels reported in the literature, these systems are not made from harmful starting materials, and no organic solvents are required during their preparation.[46–50] Our aim was to formulate systems able to act as dry systems, which can be stored by conservators in their laboratories and used, when needed, after swelling in organic solvents, without safety risks to the operators, the environment or the artifacts.

Gels were characterized before and after curing of the polyurethane network. In particular, Small-angle Neutron Scattering (SANS) was used to detail the fractality and structure of the gels at the nanoscale before and after swelling in two organic solvents commonly adopted in the cleaning of paintings. The organogels were also characterized with rheological measurements to detail their mechanical behavior. The swollen gels were then used for the removal of a photo-aged acrylic-ketonic varnish from watercolor mock-ups. Their cleaning effectiveness was evaluated under visible and ultraviolet light, as well as using FTIR 2D imaging.

## 2. Materials and methods

### 2.1. Materials

Castor oil (CO, viscosity: 2.11 $10^{-4}$ $m^2/s$ at 40 °C, Guinama) was used as received without any purification. Poly (hexamethylene diisocyanate) (PDI, viscosity: 1.3–2.2 Pa s at 25 °C, Aldrich) and polyethylene glycol (PEG, average molecular mass: 950–1050 Da, Merk) were used, as received, for the preparation of the gels.

*p*-xylene (Xyl, ReagentPlus®, 99.0 % Sigma-Aldrich), fully deuterated *p*-xylene (d-Xyl, 99.0 %, Sigma-Aldrich), *n*-pentanol (PeOH, technical grade, Carlo Erba), fully deuterated *n*-pentanol (d-PeOH, 98.0 %, Cambridge Isotope Laboratories, Inc.) were used, without further purification, as swelling solvents to generate the organogels.

### 2.2. Preparation of gels

Three series of gels were prepared using polyurethane crosslinking chemistry under mild reaction conditions. The composition of these three systems, obtained by changing the ratio between CO and PDI, or adding PEG to the mixture, is reported in Table 1. PEG was included in the formulations to investigate the

**Table 1**
Name and composition of the three gels systems.

| Name | CO (%) | PDI (%) | PEG (%) |
|---|---|---|---|
| CO82 | 82 | 18 | – |
| COPEG | 77 | 18 | 5 |
| CO84 | 84 | 16 | – |

effect of a linear polymer with terminal –OH groups in the gelation process and on the final properties of the CO gels.

The following synthetic procedure was used, regardless of the composition of the starting mixture: CO, PDI and PEG (when present) were placed in a round bottom flask at room temperature. The reaction mixture was heated at 75 °C and stirred for 45 min to obtain a pre-polymer viscous liquid. Afterwards, about 35–45 g of the pre-polymer solution was poured in 10 × 14 $cm^2$ molds, to obtain gel sheets with a thickness of 2–4 mm. The molds were cured at 60 °C. The cured gels were then removed from the molds and, when needed, immersed in organic solvents to obtain the corresponding swollen gels.

### 2.3. Characterization of gels

#### 2.3.1. ATR-FTIR measurements

Attenuated total reflection Fourier Transformation Infrared spectroscopy (ATR-FTIR) measurements were carried out to follow the curing process of the castor oil gels, using a Thermo Nicolet Nexus 870 spectrometer equipped with a liquid nitrogen-cooled HgCdTe detector and a single reflection diamond crystal ATR unit. Spectra were recorded in the 4000–650 $cm^{-1}$ range (128 scans, 2 $cm^{-1}$ spectral resolution).

#### 2.3.2. Thermogravimetric analysis (TGA)

The thermal behavior of gels was studied by TGA using an SDT Q600 TA Instrument, operating between 30 and 600 °C at a heating rate of 10 °C/min under nitrogen flow (100 mL/min). For each measurement, about 10 mg of sample was placed inside an alumina pan and analyzed. Measurements were repeated at least two times.

#### 2.3.3. Rheological characterization

Rheological measurements were carried out with a TA Instrument Hybrid Rheometer DISCOVERY HR-3, using a plate-plate geometry (flat plate 20 mm diameter) and a Peltier temperature controller. The cell was closed by lowering the head to the measuring position in the axial force-controlled mode. Each sample was loaded onto the plate, and care was taken to minimize the stress to the sample during the loading procedure. Measurements were performed at 25 °C, with no soak time and repeated at least two times. Amplitude sweep tests ($\gamma$ = 0.01–10 %; 1 Hz) were performed to determine the linear viscoelastic (LVE) region. Frequency sweep measurements were then carried out over the frequency range 0.01–10 Hz at a constant strain within LVE region.

#### 2.3.4. Small-angle Neutron scattering (SANS)

SANS experiments were conducted at the SANS-1 instrument at the Heinz-Maier-Leibnitz Zentrum (MLZ),[51,52] using three different configurations (neutron beam wavelength ($\lambda$)/sample-to-detector distances: 4.5 Å /2 m, 4.5 Å /12 m, 12 Å /12 m). Measurements were acquired in a range of scattering vectors, $q$, between 0.0014 and 0.47 $Å^{-1}$ where $q = (4\pi/\lambda)\sin\theta$, and $2\theta$ is the scattering angle. The scattering intensity was corrected for the empty cell contribution, transmission, and detector efficiency. The reduction of the data was performed using BerSANS.[53] The background from the incoherent scattering coming from each sample was determined from the analysis of the Porod asymptotic limit and subtracted from the scattering pattern. In the case of swollen samples, the contribution of the corresponding dry system was subtracted prior to fitting. Experimental data were fitted using a custom model implemented in SasView (version 5.0.3).[54] The Scattering Length Density (SLD) of the gels' components and of the deuterated solvents is reported in Table S1.

#### 2.3.5. Swelling degree of organogels

When immersed in organic solvents, the cured gels increase in size and weight. The amount of solvent absorbed by the polymeric network was measured gravimetrically at different loading times to calculate the swelling degree (SD):

$$SD(\%) = \frac{W_s - W_d}{W_d} \cdot 100 \quad (1)$$

where $W_s$ is the weight of the swollen gel at a particular time and $W_d$ is the weight of the corresponding dry gel. Measurements were repeated at least three times.

### 2.4. Cleaning tests using solvent-loaded gels

#### 2.4.1. Mock-ups preparation

Mock-ups were prepared using Winsor & Newton watercolors (Blue and Ochre). Watercolors were brushed on a canvas prepared with Bologna chalk and animal glue. After one year, the painting was varnished using an acrylic-ketonic varnish (Retoucher Vibert by J.G. LeFranc&Bourgeois). The varnished painting was artificially aged in a home-made ageing chamber equipped with three Neon Light Colour 765 BASIC Daylight Beghelli lamps (160 mW/lm, 380–700 nm) for 30 days (36 ℃, r. h. 40 %) where the sample' surface was exposed to ca. 11,000 Lux of homogeneous illumination. These conditions are meant to accelerate the natural aging that would be experienced by objects on display in museums, where illuminations of 50–100 lx are typically used.

#### 2.4.2. Cleaning tests on mock-ups

Before applicative tests, the gels were immersed in *p*-xylene (Xyl) and *n*-pentanol (PeOH) to load an appropriate amount of solvent for applicative purposes. After swelling, the gels were dried with blotting paper to remove the solvent excess from their surface and placed on the varnished surface for a variable amount of time (from 30 s to few minutes). When needed, an extremely gentle mechanical action was performed with humid cotton swabs to completely remove the residues of the swollen, softened acrylic-ketonic varnish.

#### 2.4.3. Fourier-transform infrared (FTIR) spectroscopy imaging

The 2D FTIR imaging of the painting mock-ups was carried out using a Cary 620–670 FTIR microscope, equipped with a Focal Plane Array (FPA) 128 × 128 detector (Agilent Technologies). This set-up was selected as it allows discriminating compounds with different chemical composition on a surface down to a spatial resolution of few microns, and it has been validated through several case studies to assess restoration methodologies, the degradation status and the cleaning of works of art.[31,55–58] The spectra were recorded directly on the surface of the mock-ups in reflectance mode, with open aperture and a spectral resolution of 8 $cm^{-1}$, acquiring 128 scans for each spectrum. A "single tile" map has dimensions of 700 × 700 $\mu m^2$ (corresponding to 128 × 128 pixels); each pixel has dimensions of 5.5 × 5.5 $\mu m^2$ and provides an independent spectrum, which makes thousands of independent spectra collected simultaneously on each sample. The chromatic scale of the false-color maps shows the absorbance of the mapped bands as follows: blue < green < yellow < red. To assess effective varnish removal, 2D FTIR characteristic bands of the acrylic-ketonic varnish were imaged on the surface of the mock-ups before and after application of the CO82 gels swollen in the two organic solvents.

## 3. Results and discussion

### 3.1. Synthesis of gels

Castor oil is an environmentally friendly and inexpensive vegetable oil extracted from pressed castor beans, which includes a mixture of triglycerides where about 90 % of fatty acids are ricinoleates. The latter are triglycerides containing ricinoleic acid, a quite unusual fatty acid that, having a reactive hydroxyl group on the 12th carbon available for functionalization, has been widely used for the preparation of biodegradable polymers, cosmetics, lubricants, biofuels, coatings and adhesives, and volatile organic compounds (VOCs) absorbers.[59–63].

Here, castor oil-based gels were prepared by forming a polyurethane pre-polymer under mild reaction conditions and without using any solvent (see section 2.2 for detailed information about the synthetic procedure). The pre-polymer can be cast to any desired shape and cured to obtain a biomass-derived hypercrosslinked gel that does not require any further purification, making the overall gelation process sustainable and cost effective.

The curing process was assessed by ATR-FTIR spectroscopy. Castor oil shows a broad peak in the 3650–3150 $cm^{-1}$ range, due to the presence of hydroxylated ricinoleic acid, and a characteristic peak at 1742 $cm^{-1}$ (-C═O stretching of the triglyceride ester carbonyls (Fig. 1A)).[64] The band at 3007 $cm^{-1}$ is ascribed to -C—H stretching vibrations of *cis*-double bond, whereas the band at 2925 $cm^{-1}$ and 2854 $cm^{-1}$ are characteristics of asymmetric and symmetric vibrations of aliphatic $-CH_2$ fatty acid hydrocarbon chains.[65,66] The bending of $-CH_2$ aliphatic groups (i.e. scissoring) are found at 1460 $cm^{-1}$, while the bands at 1239, 1162, 1096 and 1033 $cm^{-1}$ are due to bending vibrations of ester carbonyl group.[65,66] The = $CH_2$ wagging vibrations fall at 859 $cm^{-1}$. Finally, the band at 725 $cm^{-1}$ comes from the overlapping of $-CH_2$ rocking out of plane vibration of *cis*-disubstituted olefins, characteristics of long chain fatty acids.

In the pre-polymer mixture (yellow solid line in Fig. 1A), the peak of the isocyanate ═(-NCO) group was detected at ca. 2270 $cm^{-1}$.[67] Its intensity gradually decreases during the curing process until it becomes negligible in the spectrum of the cured gels (red solid line in Fig. 1A), confirming that all isocyanate groups reacted with the hydroxyls of castor oil after 24 h. The formation of urethane bonds in the cured samples is confirmed by several additional changes in the ATR-FTIR spectrum (see stars in Fig. 1A): the broad band between 3650 and 3150 $cm^{-1}$ becomes narrower after curing and centered at 3391 $cm^{-1}$. This absorption is commonly ascribed to the Amide A band due to –N—H stretching in urethane bonds.[67–69] In addition to that, the amide I, amide II and amide III vibrations in the urethane bonds (R-HN-C═O),[68,69] at 1688, 1521 and 1243 $cm^{-1}$ respectively, are all strongly enhanced after curing, confirming the efficient reaction between hydroxyl groups in CO and PDI that leads to the formation of carbamate bonds.[70].

To assess the curing process, changes in the viscoelastic behavior of gel's mixtures were studied through rheological measurements carried out at two different stages of gel preparation: before curing, where free ═ (-NCO) groups are still present, and after curing, in the absence of free isocyanate groups. The mechanical spectrum of the pre-polymer mixture (yellow markers in Fig. 1B) is typical of a concentrated polymeric solution, i.e. the loss modulus is significantly higher (G") than the storage modulus (G') over the entire investigated range of frequencies. The viscoelastic properties noticeably change upon curing, due to the formation of urethane bonds, leading to a significant increase in both moduli, whose average values after 24 h at 60 °C are about 140 kPa (G') and 8 kPa (G"). Moreover, in the mechanical spectrum of the cured gel, the elastic modulus is higher than the loss modulus and it is almost frequency independent, while the loss modulus shows a slight decrease with decreasing frequency, as expected for a viscoelastic solid. This means that, after the gelation process due to the formation of urethane bonds, deformations in the linear viscoelastic range are essentially elastic or recoverable.

The response of the castor oil-based gels to thermal analysis was, in all cases, characteristic of crosslinked polyurethane-based systems, supporting the conclusions on the curing process obtained by FTIR and rheological measurements. The detailed thermal behavior of the gels, as investigated by TGA, is fully reported in the SI (see additional text and Figure S1).

### 3.2. Characterization of dry systems

In the following paragraphs we discuss the characterization of the cured systems CO82 and COPEG, while additional comments and data about CO84 (which exhibit slight difference from CO82) can be found in the Supporting Information. The amplitude sweep curves of CO82 and COPEG reported in Fig. 2A are typical of chemical gels, in which *G'* is significantly higher than *G"* and both moduli are almost not affected by increasing strain. In the investigated samples, the linear viscoelastic (LVE) region is wide and covers almost the entire range of investigated strain (measurements were

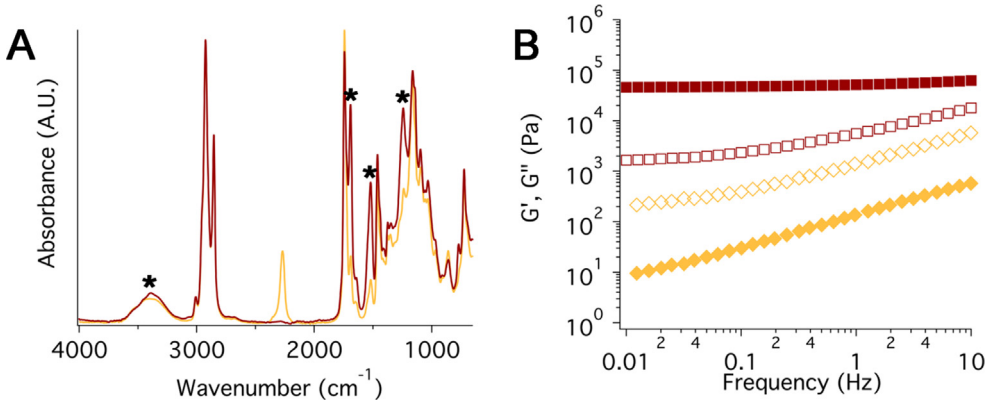


**Fig. 1.** (**A**) ATR-FTIR spectra of CO82 mixture before (yellow solid line) and after curing (red solid line). After curing, the peak of the isocyanate at ca. 2270 $cm^{-1}$ ═(-NCO) disappears as isocyanate groups react with the hydroxyl groups of castor oil. The stars highlight changes in the spectrum of the cured sample at 3391, 1688, 1521 and 1243 $cm^{-1}$, which indicate the formation of urethane bonds (see main text for the full explanation). Similar spectra (not shown) have been obtained for the other gel formulations. (**B**) Frequency sweep curves of CO82 mixture before curing (yellow diamonds) and after curing (red squares). Filled marks: storage modulus (G'); empty marks: loss modulus (G"). Error bars are comparable or smaller than the markers' size. (For interpretation of the references to color in this figure legend, the reader is referred to the web version of this article.)

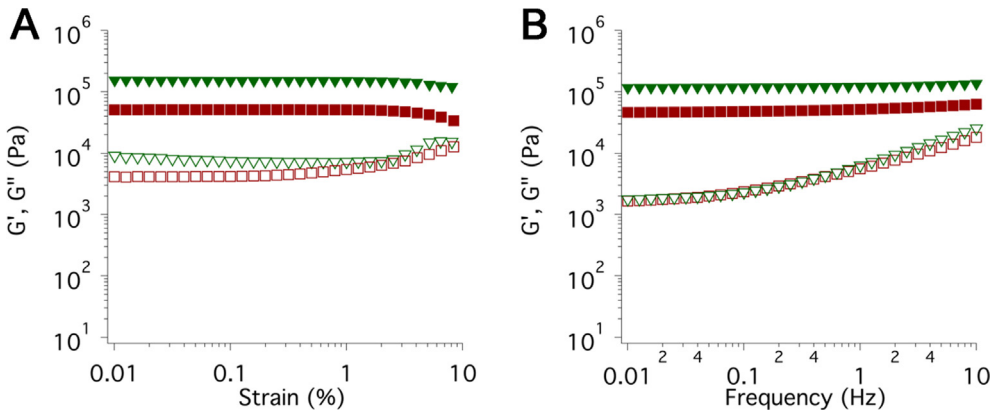


**Fig. 2.** (**A**) Amplitude sweep curves of CO82 (red squares) and COPEG (green triangles). (**B**) Frequency sweep curves of CO82 (red squares) and COPEG (green triangles). Filled marks: storage modulus (*G'*); empty marks: loss modulus (*G"*). Error bars are comparable or smaller than the markers' size. (For interpretation of the references to color in this figure legend, the reader is referred to the web version of this article.)

carried out at 1 Hz). Only at strain values close to 10 %, *G'* started to decrease, while *G"* increases. This phenomenon is preliminary to the crossover point of the two moduli that corresponds to the disruption of the network structure. The addition of a linear reactive polymeric chain (PEG), at the expense of castor oil, ends up in a significant increase in the elastic modulus. A similar trend is shown by the frequency sweep curves, acquired in the LVE region, as reported in Fig. 2B. The value of tan $\delta$, i.e. *G"*/*G'*, can be used to differentiate gel-like systems in two categories, namely, "weak" (tan $\delta$ higher > 0.1) and "strong" gels (tan $\delta$ higher < 0.1).[71–73] Regardless of their composition, all the investigated systems can be considered strong gels, as their tan $\delta$ at 1 Hz is about one order of magnitude lower than 0.1. These gels are thus expected to be easily removable in one piece from surfaces, without leaving solid residues, as opposed to weak (physical) networks, commonly used in conservation.[24,25].

SANS measurements detailed the nanostructure of the castor oil gels. The data were fitted using a custom model implemented in SasView, [54] which combines different q-dependent contributions, as follows:

$$I(q) = I_{Porod}(q) + I_{Network}(q) + I_{Excess}(q) + I_{Gaussian1}(q) + I_{Gaussian2}(q) \quad (2)$$

The first contribution describes the Porod scattering from clusters, and it was used to fit the intensity increase in the low-$q$ region, which is due to the scattering of the surface of large inhomogeneities. The equation describing this contribution is a special case of the power law model:

$$I_{Porod}(q) = \frac{I_P(0)}{q^4} \quad (3)$$

where $I_P(0)$ is the q-independent constant in the low-$q$ region and the $q$ exponent was fixed to $-4$.

The two following contributions, namely $I_{Network}$ and $I_{Excess}$, have been proposed for the fitting of inhomogeneous solids by Debye and Bueche[74] and used afterwards to model different types of gels' networks.[27,70,75–77].

The $I_{Network}$ term accounts for the scattering coming from a 3D network characterized by a correlation length, as seen in semi-dilute polymer and gel systems. This is given by:[78]

$$I_{Network}(q) = \frac{I_L(0)}{1 + (q \cdot \xi)^m} \quad (4)$$

where $I_L(0)$ is the network scattering intensity at $q$ = 0 and $\xi$ the correlation length describing the so called "blob"-size (i.e. average dimension of the characteristic mesh of the gel). The fractal dimension, $m$, varies from 1, for 1D object such as a rod, to 4 for objects with smooth surface. An exponent in the range 3–4 characterizes rough interfaces of fractal dimension $D$ with $m = 6\text{-}D$, while $m$ is 2 for pure semi-dilute polymer systems, and between 2 and 3 for "mass fractals" such as branched systems, i.e., gels, or networks. [79].

The $I_{Excess}$ contribution accounts for the scattering from inhomogeneities in the system, such as zones with higher cross-linking density or solid-like polymer domains. Typically, it refers to an excess of scattering with respect to that of the gel's network.[80] Here, the excess term is modeled by a Guinier function: [76]

$$I_{Excess} = I_G(0) \cdot exp\left[-\frac{q^2 \cdot R_g^2}{3}\right] \quad (5)$$

where $I_G(0)$ is the Guinier excess intensity at $q$ = 0 and $R_g$ is the radius of gyration of the inhomogeneities in the gel's network.

For all dry gels, SANS curves (see SI, Figure S2) show two signals in the low/medium $q$-range that are probably due to a sort of periodicity in the network that, however, cannot be fitted to the most common models for ordered objects such as spheres, lamellar stack, paracrystals, etc. These contributions were therefore modeled using standard gaussian peaks, namely $I_{Gaussian1}$ and $I_{Gaussian2}$ in Eq. (2), with the generic formula:

$$I_{GaussianX} = I_{GaX} \cdot exp\left[-\frac{0.5 \cdot (q - q_X)^2}{\sigma_X^2}\right] \quad (6)$$

where $I_{GaX}$ is the scale of the gaussian peak, centered at $q_X$ and with a standard deviation of $\sigma_X$. These contributions are not significantly affected by changes in the composition (see Supporting Information for further details).

The main fitting results are reported in Table 2, while all the parameters are included in Table S2.

The size of inhomogeneities in the gel's network, such as solid-like polymer domains, described by the gyration radius $R_g$, is not significantly affected by changes in the amount of PDI in the systems, while a slight increase in $R_g$ was obtained in the case of the addition of pre-formed linear polymer chains, i.e., PEG.

The studied samples are characterized by fractal dimension $m \sim 2.5$, indicating branched systems, i.e., gels or networks.[79] It can be concluded that the polymer chains are slightly collapsed and are in between a semi-dilute system ($m$ = 2) and a fully collapsed system describing solid-like particles ($m$ = 3). Moreover, the obtained values are in agreement with those obtained from scattering measurements performed on solvent free adhesives

**Table 2**
Main fitting parameters obtained from fitting dry gels' data to Eqs. (3)–(6).

| Sample | Fitting parameters | | | | | |
|---|---|---|---|---|---|---|
| | $I_G(0)$ | $R_g$ ± 8 Å | $I_L(0)$ | $\xi$ ± 0.5 Å | $m$ ± 0.1 | $I_G(0)/I_L(0)$ |
| CO82 | 0.25 | 76 | 0.22 | 2.1 | 2.6 | 1.14 |
| COPEG | 0.15 | 85 | 0.30 | 2.0 | 2.5 | 0.5 |

derived from castor oil and a linear hexamethylene diisocyanate (HDMI), where a fractal dimension of 2.8 was measured.[70] $\xi$ is usually associated to the distance between polymer chains, comparable to the distance between the cross-linking points, which in turn is commensurate with the mesh size.[81,82] The $\xi$ values here obtained from the fitting of the three cured gels do not seem to be affected by changes in the composition of pre-gel mixtures. The change of the crosslinker's structure from a linear (HDMI) to a branched isocyanate (PDI) results in a much smaller mesh size.

The $I_G/I_L$ ratio is proportional to the density of inhomogeneities with respect to the polymer network, and increases with the amount of isocyanates used in the pre-polymer mixture ($I_G/I_L$ = 0.24 in CO84, see Table S2, and 1.14 in CO82, see Table 2), proving that the inhomogeneities are mostly associated to the solid-like regions denser in crosslinking points.[70] The addition of PEG leads to intermediate values of $I_G/I_L$, probably due to some of the –OH terminations in the PEG chains reacting with PDI and decreasing the overall amount of crosslinking points between CO chains with respect to the CO82 case.

### 3.3. Characterization of swollen gels

One of the most interesting features of the CO-based gels here proposed is their capability of loading organic solvents in their nanosized polymeric mesh, which is indeed a key point for their use in the cleaning of works of art. To detail the changes in the nanostructure of the systems as a result of the uptake of organic solvents, gels were immersed in fully deuterated p-xylene (d-Xyl) and *n*-pentanol (d-PeOH) and then analyzed using SANS, as detailed in section 2.3.4. These two solvents were selected, as they represent two common choices in the restoration practice with opposite polar and hydrogen-bonding characters, to investigate a wide range of possible interactions with the castor oil gel networks.

SANS profiles of swollen gels were fitted with a custom model implemented in SasView, [54] which needs only two different *q*-dependent contributions, already defined in Eq. (3) and (4):

$$I(q) = I_{Porod}(q) + I_{Network}(q) + bkg \quad (7)$$

As a result of the swelling, characteristic lengths in the network increase and, as it usually happens, some of the contributions are not necessary in the fitting, either because the solid-like inhomogeneities disentangle or they swell so that their size is out of the limits of the SANS range. With the aim of detailing the changes in the network due to the sole uptake of deuterated organic solvents, the contribution of dry gels, which was only slightly visible at low q, was subtracted from the corresponding SANS curves of swollen systems before the fitting procedure. The main fitting results are reported in Table 3, while all the parameters obtained are reported in Table S3. SANS profiles of swollen CO82 and COPEG gels, together with their best fitting curves are shown in Fig. 3, while data for CO84 are included in the Supporting Information.

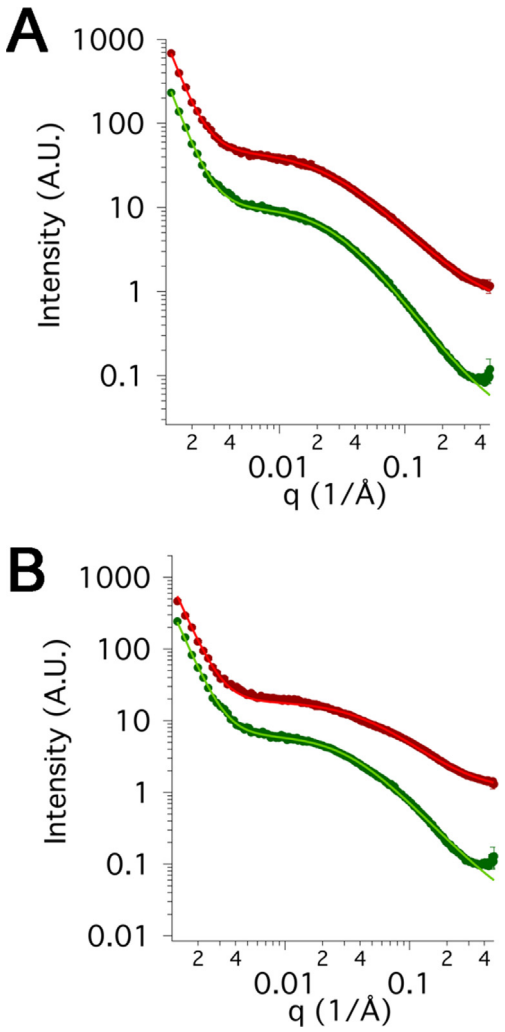


**Fig. 3.** SANS profiles of swollen gels (markers), together with their best fitting curves (solid lines). The curves were arbitrarily offset, for sake of clarity. (**A**) CO82 (red markers) and COPEG (green markers) swollen in d-PeOH. (**B**) CO82 (red markers) and COPEG (green markers) swollen in d-Xyl. (For interpretation of the references to color in this figure legend, the reader is referred to the web version of this article.)

**Table 3**
Main fitting parameters obtained from fitting swollen gels' data to Eqs. (7), together with the gel-solvent affinity ($R_a$, see Eq. (8)) and swelling degree (*SD*) values.

| Sample | Fitting parameters | | | $R_a$ | *SD* % (168 h) |
|---|---|---|---|---|---|
| | $I_L(0)$ | $\xi$ ± 3 Å | $m$ ± 0.1 | | |
| CO82-PeOH | 9.7 | 39 | 1.6 | 3.1 | 178 ± 4 |
| COPEG-PeOH | 9.9 | 38 | 1.9 | 3.4 | 170 ± 3 |
| CO82-Xyl | 3.8 | 21 | 1.7 | 9.5 | 119 ± 25 |
| COPEG-Xyl | 6.3 | 31 | 1.9 | 9.3 | 124 ± 10 |

As a result of the uptake of the organic solvents, the network scattering intensity at $q$ = 0, $I_L(0)$, is increased of about one order with respect to that of the corresponding dry systems (see Table 2 and Table S2). After swelling, the exponent $m$ obtained from the fitting of SANS curves moves from 2.5, which correspond to branched systems, to values lower than 2. It is worth recalling that the $m$ value is related to the Flory excluded volume exponent, $v$ (i.e., $m = 1/v$), that describes the interactions between the polymer chains and the solvent in which they are immersed. In particular, for fully swollen polymer chains $v$ is 3/5 ($m$ = 1.66), while a $v$ of 1/2 ($m$ = 2) is observed when the polymer is in a *theta* solvent, i.e., when chain-chain and chain-solvent interactions are equivalent; on the other hand, $v$ is 1/3 ($m$ = 3) if chain-chain interactions are favored, leading to the so-called "chain collapse".[83] Polymer chains seem to be fully swollen in samples CO82 loaded with d-PeOH and in sample CO82 loaded with d-Xyl ($m$ = 1.6–1.7). In the other systems, an intermediate situation is shown, where the highest $m$ values are displayed by COPEG swollen in d-PeOH and in d-Xyl, both of which seem to correspond to a *theta* solvent conditions for this gel formulation ($m$ close to 2).

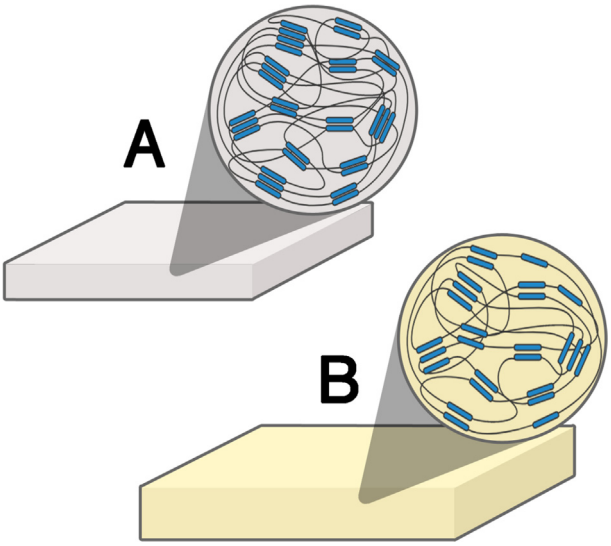


**Fig. 4.** The figure shows the increment in the nanosized mesh of the polymeric network, and the swelling of the CO gels passing from a dry system (A) to a gel loaded with an organic solvent (B).

The solvent uptake causes the blob size $\xi$ to significantly increase with respect to the dry gels. In all cases, the highest values were displayed by samples immersed in d-PeOH. These changes have been visually schematized in Fig. 4 that shows the increment in the nanosized mesh of the polymeric network, and the swelling of the gels, upon loading and confinement of the organic solvents.

To explain the difference in swollen systems, Hansen solubility parameters (HSPs) have been considered, which are a practical extension of the Hildebrand parameter to polar and hydrogen-bonding systems, primarily for polymer–liquid interactions [84–86]. According to the literature, HSPs can be used for an evaluation of gel swelling by a solvent [87]. Free-volume models can provide a more comprehensive description but contain several parameters that are not easily accessed experimentally.[88] In particular, the affinity between a polymer (1) and a solvent (2) can be calculated from their partial solubility parameters, i.e., $\delta_d$, the dispersive term, $\delta_p$, the polar term, and $\delta_h$, the hydrogen-bonding term, using a simple formula developed by Skaarup:[89]

$$R_a^2 = 4(\delta_{d1} - \delta_{d2})^2 + (\delta_{p1} - \delta_{p2})^2 + (\delta_{h1} - \delta_{h2})^2 \quad (8)$$

where the solubility parameter "distance" $R_a$ is lower in systems that are alike and higher for systems that are not similar. The factor 4 in front of the $\Delta\ \delta_d$ term has aroused controversy for decades, but theoretical reasons and experimental evidence have recently showed that it is valid.[89] In our case, the HSPs for gel components and for pure solvents were obtained from the HSPiP software - Hansen Solubility Parameters in Practice,[90] while the HSPs of gels were calculated starting from those of pure components, combining them on the basis of their volume fraction in uncured mixtures, as it commonly occurs for solvent blends (see Supporting Information). The values are reported in Table S4. Even if this approach does not take into account the newly formed bonds in the cured systems, it can provide useful data to explain the changes in the nanostructure of the gel network as a result of the uptake of different solvents.

The calculated $R_a$ between gel formulations and solvents, reported in Table 3 and in Table S5, clearly demonstrated the higher affinity of PeOH than Xyl to CO-based networks. This is in good agreement with the swelling degree (*SD*) of the gels' formulations in the two solvents after 168 h (i.e., 1 week), which are included in Table 3 and in Table S5. The *SD* values as a function of different loading times are reported in Figure S3. Interestingly, the uptake of PeOH by CO-based gels grows steadily until it reaches a plateau after about 120 h, while the loading of Xyl displays a maximum at around 24 h, followed by a decrease and a plateau at about 120 % after 5 days. It is worth noting that the

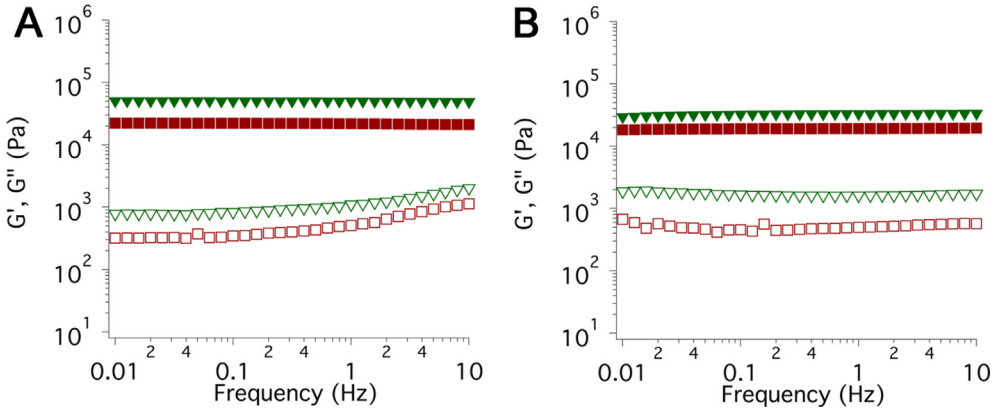


**Fig. 5.** (**A**) Frequency sweep curves of CO82 (red triangles) and COPEG (green squares) swollen in PeOH. (**B**) Frequency sweep curves of CO82 (red markers) and COPEG (green markers) swollen in Xyl. Filled marks: storage modulus (G'); empty marks: loss modulus (G''). Error bars are included in the markers. (For interpretation of the references to color in this figure legend, the reader is referred to the web version of this article.)

difference between the two series is well above the experimental error, even if the uptake of xylene shows a greater dispersion of the data.

COPEG shows the highest *m* value after swelling in PeOH, which is characteristic of partially swollen polymer coils, and the lowest increase in $\xi$ with respect to the dry system. This can be explained by the lower affinity of this formulation to the solvent, as confirmed by the highest *Ra* value in the series. *SD* data corroborate this hypothesis, being the uptake of PeOH in COPEG sample lower than those of the other systems. Moreover, it is interesting to note that the system that features the lowest amount of PDI shows the highest $\xi$ value together with a solvent uptake of about 25 % higher than the other two systems (see Supporting Information), probably because of a less entangled network. A similar situation is shown by systems swollen in Xyl, where the sample with the highest value of $\xi$ features a looser network with fewer junction points. In terms of SD, given the dispersion of the experimental data, no noticeable difference between the three gels was observed. The value of $\xi$ measured on the CO82 sample, on the other hand, is significantly lower than the other systems, probably owing to a tigh-

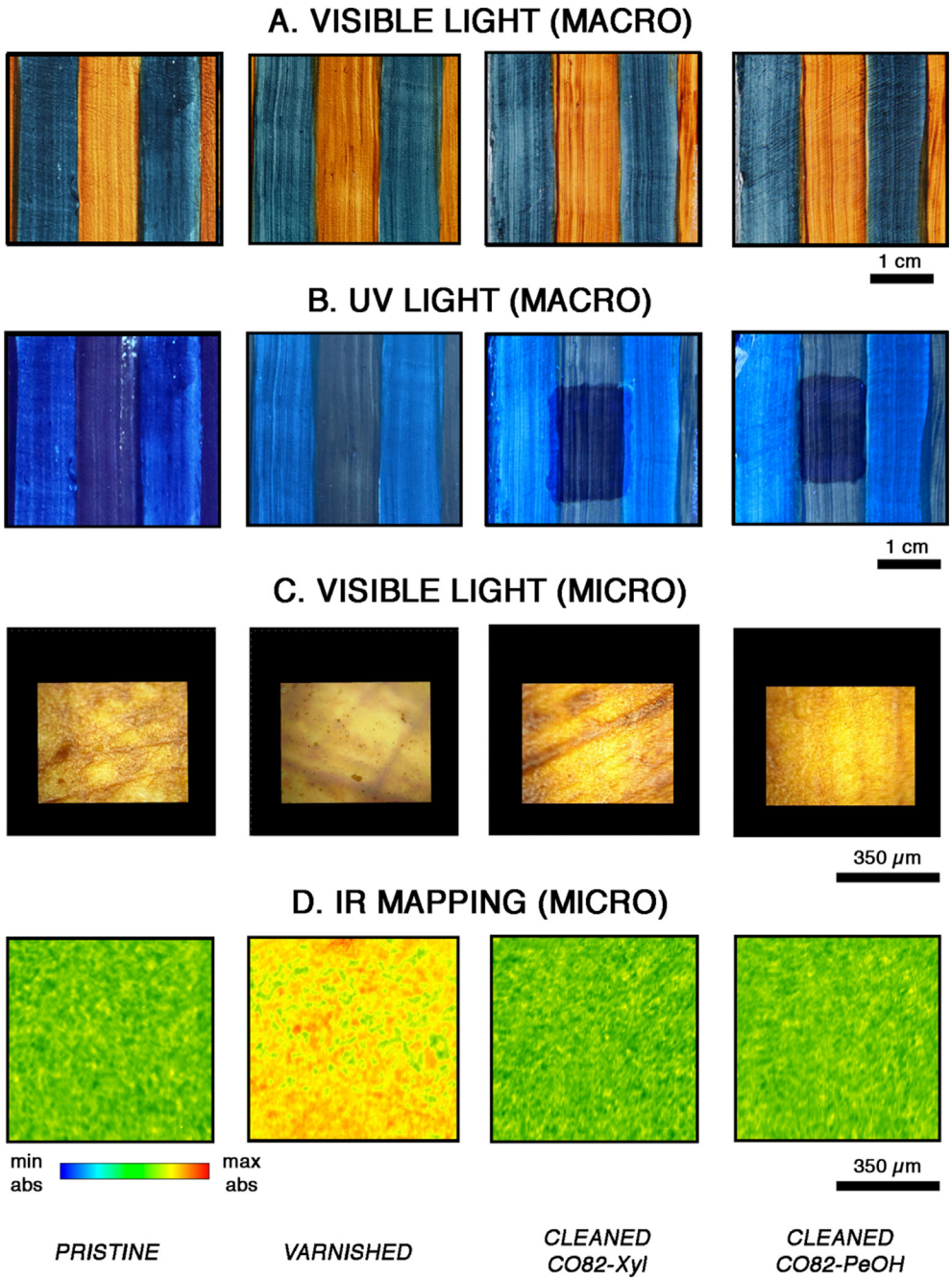


**Fig. 6.** (**A**) Pictures of mock-ups acquired under visible light on the untreated sample (pristine), after the application and aging of the acrylic-ketonic varnish (varnished), and following treatment with swollen CO82 gels (CO82 Xyl and CO82-PeOH). (**B**) Pictures of mock-ups acquired by irradiating the same samples with UV light, where the varnish shows as a matte finish on the paint surface. Dark areas in the pictures of cleaned mock-ups indicate the removal of the varnish. (**C**) Optical microscope pictures of the mock-ups. (**D**) 2D FTIR imaging of the same samples obtained by mapping the 1860–1685 $cm^{-1}$ region, where the characteristic absorption of the acrylic-ketonic varnish (C=O stretching) falls (see Figure S4 for representative IR spectra of the different samples); an average spectrum of the pristine, unvarnished watercolor surface was subtracted from each tile's set of spectra, before imaging the 1860–1685 $cm^{-1}$ region.

ter network that comes from the higher amount of PDI used in the synthesis. Finally, as indicated above, some of the –OH terminations in PEG chains probably react with PDI, which decreases the overall number of crosslinking points between CO chains, ending in a higher $\xi$ value with respect to CO82.

As shown in the frequency sweep curves reported in Fig. 5, following the uptake of the two solvents, *G'* and *G"* decrease significantly from the dry systems (Fig. 2B). In particular, the loss modulus *G"* decreases by at least an order of magnitude and is almost frequency independent, as expected for a swollen gel. This is a clear indication that the systems become more compliant, and that the crossover between the two moduli is shifted to higher frequencies, outside the instrumental limits. This is due to a plasticizing effect of the solvent associated to the increase in blob size showed by SANS investigations and explains the mechanical spectra of the gels that become macroscopically less rigid. Rheological investigations also confirm the effect of composition on the interactions with solvents, as already suggested by the scattering measurements: the reduction in the PDI amount decreases *G'* and *G"* after swelling, as a result of a less entangled network (see Supporting Information). On the other hand, the system with PEG has a significantly higher *G'* than the other systems both before and after swelling. In particular, PeOH seems to have slightly less affinity to COPEG, as also indicated by SANS data. Regardless the solvent used for swelling, CO82 displays values of *G'* and *G"* in line with those of hydrogels commonly used for the conservation of works of art, which are deemed as optimal values to allow easy handling during application and a safe removal after cleaning procedure. [29,34] Therefore, this system shows peculiar features that can be exploited for the conservation (cleaning) of art.

### 3.4. Application of swollen organogels

To the best of our knowledge, the proposed CO-based gels are the first organogels developed for the cleaning of works of art that are synthesized without solvents or diluents. This implies that the gels, which are formulated as dry systems, can be stored by conservators in their laboratories without posing a risk to the safety of the operators and used, when needed, after swelling in the preferred organic solvents. The organogels previously reported in the literature are synthesized using solvents and must be stored in ventilated cabinet before use, as they cannot be dried after the preparation without irreversible shrinkage of their porous structure, making their application less feasible. Therefore, the solvent to be used for application must be either selected before the synthetic procedure or exchanged before application.[46,47,49,91].

For applicative tests, the gels were immersed in *p*-xylene (Xyl) for 0.5 h and in *n*-pentanol (PeOH) for 4 h to load an appropriate amount of solvent (weight increase of about 50 %). After swelling, the gels were applied on the varnished surface for a variable amount of time (from 30 s to few minutes).

As clearly shown by pictures of the mock-ups under visible light (Fig. 6A and 6C), the acrylic-ketonic varnish coat produces some aesthetic alteration of the watercolors; the varnish shows under ultraviolet (UV) light as a matte finish all over the paint layer (see Fig. 6B).

The application of swollen CO82 gels allowed recovering the original look and gloss of the surface. 2D FTIR imaging of the mock-ups is shown in Fig. 6D. First, a "single tile" set of spectra ($700 \times 700$ μm$^2$, $128 \times 128$ independent spectra) was acquired on the unvarnished mock-up, and an average reflectance spectrum of the watercolor surface was obtained from 15 locations (pixels, each of $5.5 \times 5.5$ μm$^2$) homogeneously distributed over that area to account for spectral variations owed to surface roughness and compositional inhomogeneities. The latter are typically due to the presence of additives such as fillers, extenders and dispersing agents (e.g. calcium carbonate, ox gall, starch) commonly used in watercolor paints.[92].

The average spectrum was subtracted from the entire unvarnished tile set, obtaining reference spectra that reasonably exhibit only weak or no absorptions. The 1860–1685 cm$^{-1}$ region of this reference tile was then imaged to produce the "*PRISTINE*" false colors map in Fig. 6D, where green (low-absorbance) pixels dominate, and only sparse spots with slightly higher absorption (yellow pixels) are randomly distributed over the surface. Subtracting the same average spectrum from a tile acquired on the varnished (and aged) mock-up, yielded spectra with a clear absorption band in the 1860–1685 cm$^{-1}$ region, owed to the C=O stretching peak of the acrylic-ketonic varnish. The corresponding false color map ("*VARNISHED*" in Fig. 6D) is indeed dominated by red and orange (high absorbance) pixels. When the same elaboration is repeated on varnished mock-ups treated with CO82 Xyl or CO82-PeOH gels, the same pattern as for the unvarnished watercolor surface is obtained in the false color maps ("*CLEANED CO82-Xyl*" and "*CLEANED CO82-PeOH*" in Fig. 6D), confirming that varnish removal occurred homogeneously even at the micro-scale. Representative Reflectance spectra of the unvarnished, varnished, and cleaned mock-ups (before subtraction of the average unvarnished spectrum) are showed in Figure S4 for additional comparison. No absorption characteristic of the CO gel (e.g. carbonyl stretching in the 1780–1735 cm$^{-1}$ region) was observed in the spectra of the cleaned mock-ups (see also Figure S4), indicating that no measurable gel residues were left on the surface after cleaning. It is worth noticing that the detection limit of the FPA detector in Reflectance mode, using the same setup, was recently proved to be < 0.6 pg/pixel, i.e. < 0.02 pg/μm$^2$.[31].

## 4. Conclusions

Castor oil (CO)-based systems were specifically designed to address the challenge of cleaning artistic surfaces that cannot withstand the application of water. In such contexts, when conservators frequently opt for organic solvents over aqueous formulations, the new systems proved to be highly effective tools, complementary to the chemical hydrogel networks that we previously demonstrated as the most performing systems nowadays available. [27–31,34].

Our starting hypothesis was that the CO networks, formulated as dry systems, could upload organic solvents commonly used in restoration and confine them in the polymeric mesh, and then release the fluids at controlled rate to remove varnishes from painted layers.

The overall synthetic route, based on polyurethane crosslinking chemistry, is cost-effective and ecofriendly, as the starting materials are not harmful, and organic solvents are not used during the preparation, differently from other organogels.[46,47,49] The gels are obtained as dry systems that can be loaded with organic solvents when needed, allowing for an easy storage (i.e. outside ventilated cabinets).

Changes in the composition of the pre-gel mixtures, e.g. tuning the CO-isocyanate ratio or partially substituting CO with polyethylene glycol, affects the overall number of crosslinking points between CO chains. This, in turn, results in differences in the mechanical behavior, as evidenced by rheological measurements, and in the nanostructure, as detailed by SANS measurements. The different affinity between the gel network and solvents can be used to explain the difference between swollen systems in terms of elastic and loss moduli, of network organization at the nanoscale, and swelling degree. The swollen CO gels are transparent, which is advantageous to check their step-by-step cleaning action, and retain their good mechanical properties. Loading and

confinement of the solvents in the nanosized polymeric mesh of the gels is likely key to explain their optimal cleaning effectiveness: the systems are highly retentive, allowing for the controlled release of solvents over delicate paint layers. This is a crucial feature, as modern and contemporary paintings frequently exhibit pronounced sensitiveness to solvents and cleaning fluids. The CO gels represent thus a promising new tool to expand the palette of art conservators, and explore new possibilities in the use of hypercrosslinked resins, a promising class of materials that already showed great applicative potential as adsorbers.[63,93–95].

Considering that nowadays only few options are available for the cleaning of such sensitive works of art, the results here presented are a significant step forward in the development of feasible and "green" solutions for art conservation, fostering the transfer of our heritage to future generations. Future work will involve exploring different crosslinkers to improve the characteristics of the CO gels, verifying their affinity to other classes of solvents, and testing these gels on works of art belonging to the modern/contemporary art production; the latter typically exhibits problematic and delicate cleaning requirements, which prevent the use of traditional non-confined or thickened solvents.

## Funding

CSGI, the Italian Ministry MUR under agreement PRIN-2017249YEF and the European Union (GREENART project, Horizon Europe research and innovation program under grant agreement no. 101060941) are gratefully acknowledged for financial support. Views and opinions expressed are however those of the author(s) only and do not necessarily reflect those of the European Union or the European Research Executive Agency (REA). Neither the European Union nor the granting authority can be held responsible for them.

## CRediT authorship contribution statement

**Giovanna Poggi:** Data curation, Investigation, Methodology, Visualization, Writing – original draft, Writing – review & editing. **Harshal D. Santan:** Investigation. **Johan Smets:** Funding acquisition. **David Chelazzi:** Investigation, Methodology, Writing – original draft, Writing – review & editing. **Daria Noferini:** Investigation. **Maria Laura Petruzzellis:** . **Luciano Pensabene Buemi:** . **Emiliano Fratini:** Supervision, Conceptualization, Data curation, Writing – review & editing. **Piero Baglioni:** Supervision, Funding acquisition, Conceptualization, Writing – review & editing.

## Data availability

Data will be made available on request.

## Declaration of Competing Interest

The authors declare that they have no known competing financial interests or personal relationships that could have appeared to influence the work reported in this paper.

## Acknowledgements

PB and EF dedicate this work to the memory of Sow-Hsin Chen, a profound scientist and a dedicated mentor.

This work benefited from the use of the SasView application, originally developed under NSF award DMR-0520547. SasView contains code developed with funding from the European Union's Horizon 2020 research and innovation programme under the SINE2020 project, grant agreement No 654000. This work is based upon experiments performed at the SANS-1 instrument operated by TUM at the Heinz Maier-Leibnitz Zentrum (MLZ), Garching, Germany. Dr. Sebastian Bush is kindly acknowledged for helping with SANS experiments.

## Appendix A. Supplementary material

Supplementary data to this article can be found online at https://doi.org/10.1016/j.jcis.2023.01.119.

## References

[1] M. Lhermitte, B. Perrin, L. Melbouci, Measuring cultural and creative markets in the EU, EY. (2014) 100. http://www.creatingeurope.eu/en/wp-content/uploads/2014/11/study-full-en.pdf.
[2] N. Stanley-Price, ed., Cultural Heritage in Postwar Recovery Paper from ICCROM FORUM held on October 4-6, 2005, ICCROM, Rome, 2007.
[3] C. Holtorf, The Changing Contribution of Cultural Heritage to Society, Museum Int. 63 (2011) 8–16, https://doi.org/10.1111/j.1468-0033.2012.01758.x.
[4] C. Dümcke, M. Gnedovsky, The Social and Economic Value of Cultural Heritage: Literature Review, 2013. https://www.interarts.net/descargas/interarts2557.pdf.
[5] P. Baglioni, E. Carretti, D. Chelazzi, Nanomaterials in art conservation, Nat. Nanotechnol. 10 (2015) 287–290, https://doi.org/10.1038/nnano.2015.38.
[6] C. Miliani, F. Rosi, B.G. Brunetti, A. Sgamellotti, In Situ Noninvasive Study of Artworks: The MOLAB Multitechnique Approach, Acc. Chem. Res. 43 (2010) 728–738, https://doi.org/10.1021/ar100010t.
[7] D. Gavrilov, R.G. Maev, D.P. Almond, A review of imaging methods in analysis of works of art: Thermographic imaging method in art analysis, Can. J. Phys. 92 (2014) 341–364, https://doi.org/10.1139/cjp-2013-0128.
[8] F. Vanmeert, E. Hendriks, G. Van der Snickt, L. Monico, J. Dik, K. Janssens, Chemical Mapping by Macroscopic X-ray Powder Diffraction (MA-XRPD) of Van Gogh's Sunflowers : Identification of Areas with Higher Degradation Risk, Angew. Chemie Int. Ed. 57 (2018) 7418–7422, https://doi.org/10.1002/anie.201713293.
[9] M. Baglioni, G. Poggi, D. Chelazzi, P. Baglioni, Advanced Materials in Cultural Heritage Conservation, Molecules 26 (2021) 3967, https://doi.org/10.3390/molecules26133967.
[10] M. Leona, K. Fukunaga, H. Liang, P. Baglioni, G. Festa, V. Levchenko, From physics to art and back, Nat. Rev. Phys. 3 (2021) 681–684, https://doi.org/10.1038/s42254-021-00362-x.
[11] K.T. Faber, F. Casadio, A. Masic, L. Robbiola, M. Walton, Looking Back, Looking Forward: Materials Science in Art, Archaeology, and Art Conservation, Annu. Rev. Mater. Res. 51 (2021) 435–460, https://doi.org/10.1146/annurev-matsci-080819-013103.
[12] P. Baglioni, D. Chelazzi, R. Giorgi, G. Poggi, Colloid and materials science for the conservation of cultural heritage: Cleaning, consolidation, and deacidification, Langmuir 29 (2013) 5110–5122, https://doi.org/10.1021/la304456n.
[13] D. Chelazzi, R. Giorgi, P. Baglioni, Microemulsions, Micelles, and Functional Gels: How Colloids and Soft Matter Preserve Works of Art, Angew. Chemie Int. Ed. 57 (2018) 7296–7303, https://doi.org/10.1002/anie.201710711.
[14] D. Chelazzi, R. Bordes, R. Giorgi, K. Holmberg, P. Baglioni, The use of surfactants in the cleaning of works of art, Curr. Opin. Colloid Interface Sci. 45 (2020) 108–123, https://doi.org/10.1016/j.cocis.2019.12.007.
[15] P. Baglioni, D. Chelazzi, How Science Can Contribute to the Remedial Conservation of Cultural Heritage, Chem. – A Eur. J. 27 (2021) 10798–10806, https://doi.org/10.1002/chem.202100675.
[16] E. Carretti, G. Poggi, E. Ghelardi, F. Porpora, A. Magnani, E. Fratini, L. Dei, M. Consumi, Nanostructured fluids confined into Highly Viscous Polymeric Dispersions as cleaning tools for artifacts: A rheological, SAXS, DSC and TOF-SIMS study, Colloids Surfaces A Physicochem. Eng. Asp. 646 (2022), https://doi.org/10.1016/j.colsurfa.2022.128968 128968.
[17] C. Mazzuca, L. Micheli, M. Carbone, F. Basoli, E. Cervelli, S. Iannuccelli, S. Sotgiu, A. Palleschi, Gellan hydrogel as a powerful tool in paper cleaning process: A detailed study, J. Colloid Interface Sci. 416 (2014) 205–211, https://doi.org/10.1016/j.jcis.2013.10.062.
[18] Y. Cao, A. Salvini, M. Camaiti, One-step fabrication of robust and durable superamphiphobic, self-cleaning surface for outdoor and in situ application on building substrates, J. Colloid Interface Sci. 591 (2021) 239–252, https://doi.org/10.1016/j.jcis.2021.02.001.
[19] F.C. Izzo, K.J. van den Berg, H. van Keulen, B. Ferriani, E. Zendri, Modern Oil Paints – Formulations, Organic Additives and Degradation: Some Case Studies, in: K.J. Van der Berg, A. Burnstock, M. De Keijzer, J. Krueger, T. Learner, A. De Tagle, G. Heydenreich (Eds.), Issues Contemp. Oil Paint, Springer International Publishing, Cham, 2014: pp. 75–104. 10.1007/978-3-319-10100-2_5.
[20] T.J.S. Learner, Analysis of Modern Paints, Getty Conservation Institute, Los Angeles, USA, 2004.
[21] A. Burnstock, K.J. van der Berg, S. de Groot, L. Wijnberg, An investigation of water-sensitive oil paints in 20th century paintings, in: T.J.S. Learner, P. Smithen, J. Krueger, M.R. Shilling (Eds.), Mod. Paint. Uncovered Proc. from Mod. Paint. Uncovered Symp., The Getty Conservation Institute, Los Angeles, USA, 2007: pp. 177–188.

[22] B. Ormsby, T. Learner, The effects of wet surface cleaning treatments on acrylic emulsion artists' paints – a review of recent scientific research, Stud. Conserv. 54 (2009) 29–41, https://doi.org/10.1179/sic.2009.54.Supplement-1.29.
[23] R. Wolbers, Cleaning Painted Surfaces: Aqueous Methods, Archetype Books, London, 2000. http://www.amazon.com/dp/1873132360.
[24] D. Stulik, D. Miller, H. Khanjian, N. Khandekar, R. Wolbers, J. Carlson, W.C. Petersen, Solvent Gels for the Cleaning of Works of Art: The Residue Question, The Getty Conservation Institute - J. Paul Getty Trust, Los Angeles, USA, CA, USA, 2004. http://books.google.it/books?id=G7vmQleOOzwC.
[25] A. Casoli, Z. Di Diego, C. Isca, Cleaning painted surfaces: evaluation of leaching phenomenon induced by solvents applied for the removal of gel residues, Environ. Sci. Pollut. Res. 21 (2014) 13252–13263, https://doi.org/10.1007/s11356-014-2658-5.
[26] R.L. Feller, M. Wilt, Evaluation of Cellulose Ethers for Conservation, Getty Conservation Institute, Marina del Rey, California, USA, 1990.
[27] J.A.L. Domingues, N. Bonelli, R. Giorgi, E. Fratini, F. Gorel, P. Baglioni, Innovative Hydrogels Based on Semi-Interpenetrating p(HEMA)/PVP Networks for the Cleaning of Water-Sensitive Cultural Heritage Artifacts, Langmuir 29 (2013) 2746–2755, https://doi.org/10.1021/la3048664.
[28] R. Mastrangelo, C. Montis, N. Bonelli, P. Tempesti, P. Baglioni, Surface cleaning of artworks: structure and dynamics of nanostructured fluids confined in polymeric hydrogel networks, Phys. Chem. Chem. Phys. 19 (2017) 23762–23772, https://doi.org/10.1039/c7cp02662e.
[29] C. Mazzuca, G. Poggi, N. Bonelli, L. Micheli, P. Baglioni, A. Palleschi, Innovative chemical gels meet enzymes: A smart combination for cleaning paper artworks, J. Colloid Interface Sci. 502 (2017) 153–164, https://doi.org/10.1016/j.jcis.2017.04.088.
[30] N. Bonelli, G. Poggi, D. Chelazzi, R. Giorgi, P. Baglioni, Poly(vinyl alcohol)/poly (vinyl pyrrolidone) hydrogels for the cleaning of art, J. Colloid Interface Sci. 536 (2019) 339–348, https://doi.org/10.1016/j.jcis.2018.10.025.
[31] R. Mastrangelo, D. Chelazzi, G. Poggi, E. Fratini, L. Pensabene Buemi, M.L. Petruzzellis, P. Baglioni, Twin-chain polymer hydrogels based on poly(vinyl alcohol) as new advanced tool for the cleaning of modern and contemporary art, Proc. Natl. Acad. Sci. 117 (2020) 7011–7020, https://doi.org/10.1073/pnas.1911811117.
[32] V. Rosciardi, D. Chelazzi, P. Baglioni, "Green" biocomposite Poly (vinyl alcohol)/starch cryogels as new advanced tools for the cleaning of artifacts, J. Colloid Interface Sci. 613 (2022) 697–708, https://doi.org/10.1016/j.jcis.2021.12.145.
[33] M. Baglioni, G. Poggi, R. Giorgi, P. Rivella, T. Ogura, P. Baglioni, Selective removal of over-paintings from "Street Art" using an environmentally friendly nanostructured fluid loaded in highly retentive hydrogels, J. Colloid Interface Sci. 595 (2021) 187–201, https://doi.org/10.1016/j.jcis.2021.03.054.
[34] M. Baglioni, J.A.L. Domingues, E. Carretti, E. Fratini, D. Chelazzi, R. Giorgi, P. Baglioni, Complex Fluids Confined into Semi-interpenetrated Chemical Hydrogels for the Cleaning of Classic Art: A Rheological and SAXS Study, ACS Appl. Mater. Interfaces. 10 (2018) 19162–19172, https://doi.org/10.1021/acsami.8b01841.
[35] J. Siddiqui, M. Taheri, A.U. Alam, M.J. Deen, Nanomaterials in Smart Packaging Applications: A Review, Small 18 (2022) 2101171, https://doi.org/10.1002/smll.202101171.
[36] Y. Xu, H. Zhu, A. Denduluri, Y. Ou, N.A. Erkamp, R. Qi, Y. Shen, T.P.J. Knowles, Recent Advances in Microgels: From Biomolecules to Functionality, Small 18 (2022) 2200180, https://doi.org/10.1002/smll.202200180.
[37] Z.S. Nishat, T. Hossain, M.N. Islam, H. Phan, M.A. Wahab, M.A. Moni, C. Salomon, M.A. Amin, A.A.I. Sina, M.S.A. Hossain, Y.V. Kaneti, Y. Yamauchi, M.K. Masud, Hydrogel Nanoarchitectonics: An Evolving Paradigm for Ultrasensitive Biosensing, Small 18 (2022) 2107571, https://doi.org/10.1002/smll.202107571.
[38] E. Miyako, H. Nagata, K. Hirano, T. Hirotsu, Photodynamic Thermoresponsive Nanocarbon-Polymer Gel Hybrids, Small 4 (2008) 1711–1715, https://doi.org/10.1002/smll.200800601.
[39] Q. He, Y. Liao, J. Zhang, X. Yao, W. Zhou, Y. Hong, H. Ouyang, "All-in-One" Gel System for Whole Procedure of Stem-Cell Amplification and Tissue Engineering, Small 16 (2020) 1906539, https://doi.org/10.1002/smll.201906539.
[40] L. Zhang, X. Wang, T. Wang, M. Liu, Tuning Soft Nanostructures in Self-assembled Supramolecular Gels: From Morphology Control to Morphology-Dependent Functions, Small 11 (2015) 1025–1038, https://doi.org/10.1002/smll.201402075.
[41] M. Melo, S. Bracci, M. Camaiti, O. Chiantore, F. Piacenti, Photodegradation of acrylic resins used in the conservation of stone, Polym. Degrad. Stab. 66 (1999) 23–30, https://doi.org/10.1016/S0141-3910(99)00048-8.
[42] O. Chiantore, M. Lazzari, Photo-oxidative stability of paraloid acrylic protective polymers, Polymer (Guildf). 42 (2001) 17–27, https://doi.org/10.1016/S0032-3861(00)00327-X.
[43] M.T. Doménech-Carbó, D.J. Yusá-Marco, G. Bitossi, M.F. Silva, X. Mas-Barberá, L. Osete-Cortina, Study of ageing of ketone resins used as picture varnishes by FTIR spectroscopy, UV–Vis spectrophotometry, atomic force microscopy and scanning electron microscopy X-ray microanalysis, Anal. Bioanal. Chem. 391 (2008) 1351–1359, https://doi.org/10.1007/s00216-008-1864-8.
[44] Q. Shang, J. Cheng, L. Hu, C. Bo, X. Yang, Y. Hu, C. Liu, Y. Zhou, Bio-inspired castor oil modified cellulose aerogels for oil recovery and emulsion separation, Colloids Surfaces A Physicochem. Eng. Asp. 636 (2022), https://doi.org/10.1016/j.colsurfa.2021.128043 128043.
[45] W. He, H. Huang, L. Xie, C. Wang, J. Yu, S. Lu, H. Fan, The influence of self-crosslinked epoxidized castor oil on the properties of Poly (lactic acid) via dynamic vulcanization: Toughening effect, thermal properties and structures, Colloids Surfaces A Physicochem. Eng. Asp. 630 (2021), https://doi.org/10.1016/j.colsurfa.2021.127517 127517.
[46] P. Baglioni, N. Bonelli, D. Chelazzi, A. Chevalier, L. Dei, J. Domingues, E. Fratini, R. Giorgi, M. Martin, Organogel formulations for the cleaning of easel paintings, Appl. Phys. A. 121 (2015) 857–868, https://doi.org/10.1007/s00339-015-9364-0.
[47] M.D. Pianorsi, M. Raudino, N. Bonelli, D. Chelazzi, R. Giorgi, E. Fratini, P. Baglioni, Organogels for the cleaning of artifacts, Pure Appl. Chem. (2017) 3–17, https://doi.org/10.1515/pac-2016-0908.
[48] T.T. Duncan, B.H. Berrie, R.G. Weiss, Soft, Peelable Organogels from Partially Hydrolyzed Poly(vinyl acetate) and Benzene-1,4-diboronic Acid: Applications to Clean Works of Art, ACS Appl. Mater. Interfaces. 9 (2017) 28069–28078, https://doi.org/10.1021/acsami.7b09473.
[49] P. Ferrari, D. Chelazzi, N. Bonelli, A. Mirabile, R. Giorgi, P. Baglioni, Alkyl carbonate solvents confined in poly (ethyl methacrylate) organogels for the removal of pressure sensitive tapes (PSTs) from contemporary drawings, J. Cult. Herit. 34 (2018) 227–236, https://doi.org/10.1016/j.culher.2018.05.009.
[50] J. Yiming, G. Sciutto, S. Prati, E. Catelli, M. Galeotti, S. Porcinai, L. Mazzocchetti, C. Samorì, P. Galletti, L. Giorgini, E. Tagliavini, R. Mazzeo, A new bio-based organogel for the removal of wax coating from indoor bronze surfaces, Herit. Sci. 7 (2019) 34, https://doi.org/10.1186/s40494-019-0276-8.
[51] A. Heinemann, S. Mühlbauer, SANS-1: Small angle neutron scattering, J. Large-Scale Res. Facil. JLSRF. 1 (2015) A10. 10.17815/jlsrf-1-32.
[52] S. Mühlbauer, A. Heinemann, A. Wilhelm, L. Karge, A. Ostermann, I. Defendi, A. Schreyer, W. Petry, R. Gilles, The new small-angle neutron scattering instrument SANS-1 at MLZ—characterization and first results, Nucl. Instruments Methods Phys. Res. Sect. A Accel. Spectrometers, Detect. Assoc. Equip. 832 (2016) 297–305, https://doi.org/10.1016/j.nima.2016.06.105.
[53] U. Keiderling, The new "BerSANS-PC" software for reduction and treatment of small angle neutron scattering data, Appl. Phys. A Mater. Sci. Process. 74 (2002) s1455–s1457, https://doi.org/10.1007/s003390201561.
[54] http://www.sasview.org/, (n.d.).
[55] D. Badillo-Sanchez, D. Chelazzi, R. Giorgi, A. Cincinelli, P. Baglioni, Characterization of the secondary structure of degummed Bombyx mori silk in modern and historical samples, Polym. Degrad. Stab. 157 (2018) 53–62, https://doi.org/10.1016/j.polymdegradstab.2018.09.022.
[56] D. Badillo-Sanchez, D. Chelazzi, R. Giorgi, A. Cincinelli, P. Baglioni, Understanding the structural degradation of South American historical silk: A Focal Plane Array (FPA) FTIR and multivariate analysis, Sci. Rep. 9 (2019) 17239, https://doi.org/10.1038/s41598-019-53763-5.
[57] L. Pensabene Buemi, M.L. Petruzzellis, D. Chelazzi, M. Baglioni, R. Mastrangelo, R. Giorgi, P. Baglioni, Twin-chain polymer networks loaded with nanostructured fluids for the selective removal of a non-original varnish from Picasso's "L'Atelier" at the Peggy Guggenheim Collection, Venice, Herit. Sci. 8 (2020) 77, https://doi.org/10.1186/s40494-020-00420-0.
[58] C. Cianci, D. Chelazzi, G. Poggi, F. Modi, R. Giorgi, M. Laurati, Hybrid fibroin-nanocellulose composites for the consolidation of aged and historical silk, Colloids Surfaces A Physicochem. Eng. Asp. 634 (2022), https://doi.org/10.1016/j.colsurfa.2021.127944 127944.
[59] Y. Xia, R.C. Larock, Vegetable oil-based polymeric materials: synthesis, properties, and applications, Green Chem. 12 (2010) 1893, https://doi.org/10.1039/c0gc00264j.
[60] K.R. Kunduru, A. Basu, M. Haim Zada, A.J. Domb, Castor Oil-Based Biodegradable Polyesters, Biomacromolecules 16 (2015) 2572–2587, https://doi.org/10.1021/acs.biomac.5b00923.
[61] A. Shirke, B. Dholakiya, K. Kuperkar, Novel applications of castor oil based polyurethanes: a short review, Polym. Sci. Ser. B. 57 (2015) 292–297, https://doi.org/10.1134/S1560090415040132.
[62] E.B. Mubofu, Castor oil as a potential renewable resource for the production of functional materials, Sustain. Chem. Process. 4 (2016) 11, https://doi.org/10.1186/s40508-016-0055-8.
[63] A. Zuliani, D. Bandelli, D. Chelazzi, R. Giorgi, P. Baglioni, Environmentally friendly ZnO/Castor oil polyurethane composites for the gas-phase adsorption of acetic acid, J. Colloid Interface Sci. 614 (2022) 451–459, https://doi.org/10.1016/j.jcis.2022.01.123.
[64] H. Li, S. Niu, C. Lu, Pyrolysis Characteristics of Castor Oil through Thermogravimetric Coupled with Fourier Transform Infrared Spectroscopy, Procedia Eng. 205 (2017) 3705–3710, https://doi.org/10.1016/j.proeng.2017.10.292.
[65] S.T.H. Sherazi, A. Kandhro, S.A. Mahesar, M.I. Bhanger, M.Y. Talpur, S. Arain, Application of transmission FT-IR spectroscopy for the trans fat determination in the industrially processed edible oils, Food Chem. 114 (2009) 323–327, https://doi.org/10.1016/j.foodchem.2008.09.058.
[66] S.A. Mahesar, S.T.H. Sherazi, A.A. Kandhro, M.I. Bhanger, A.R. Khaskheli, M.Y. Talpur, Evaluation of important fatty acid ratios in poultry feed lipids by ATR FTIR spectroscopy, Vib. Spectrosc. 57 (2011) 177–181, https://doi.org/10.1016/j.vibspec.2011.06.009.
[67] S. Ibrahim, A. Ahmad, N.S. Mohamed, Synthesis and characterization of castor oil-based polyurethane for potential application as host in polymer electrolytes, Bull. Mater. Sci. 38 (2015) 1155–1161, https://doi.org/10.1007/s12034-015-0995-8.

[68] C. Zhang, Z. Ren, Z. Yin, H. Qian, D. Ma, Amide II and Amide III Bands in Polyurethane Model Soft and Hard Segments, Polym. Bull. 60 (2008) 97–101, https://doi.org/10.1007/s00289-007-0837-y.
[69] G.G. Suchkova, L.I. Maklakov, Amide bands in the IR spectra of urethanes, Vib. Spectrosc. 51 (2009) 333–339, https://doi.org/10.1016/j.vibspec.2009.09.002.
[70] H.D. Santan, C. James, E. Fratini, I. Martínez, C. Valencia, M.C. Sánchez, J.M. Franco, Structure-property relationships in solvent free adhesives derived from castor oil, Ind. Crops Prod. 121 (2018) 90–98, https://doi.org/10.1016/j.indcrop.2018.05.012.
[71] S.B. Ross-Murphy, Structure–property relationships in food biopolymer gels and solutions, J. Rheol. (N. Y. N. Y) 39 (1995) 1451–1463, https://doi.org/10.1122/1.550610.
[72] I.S. Chronakis, L. Piculell, J. Borgstriim, Rheology of kappa-carrageenan in mixtures of sodium and cesium iodide : two types of gels, Carbohydr. Polym. 31 (1996) 215–225.
[73] S. Ikeda, K. Nishinari, " Weak Gel " -Type Rheological Properties of Aqueous Dispersions of Nonaggregated K -Carrageenan Helices, J. Agric. Food Chem. 49 (2001) 4436–4441, https://doi.org/10.1021/jf0103065.
[74] P. Debye, A.M. Bueche, Scattering by an Inhomogeneous Solid, J. Appl. Phys. 20 (1949) 518–525, https://doi.org/10.1063/1.1698419.
[75] S. Mallam, F. Horkay, A.M. Hecht, A.R. Rennie, E. Geissler, Microscopic and macroscopic thermodynamic observations in swollen poly(dimethylsiloxane) networks, Macromolecules 24 (1991) 543–548, https://doi.org/10.1021/ma00002a031.
[76] M. Shibayama, T. Tanaka, C.C. Han, Small angle neutron scattering study on poly(N-isopropyl acrylamide) gels near their volume-phase transition temperature, J. Chem. Phys. 97 (1992) 6829–6841, https://doi.org/10.1063/1.463636.
[77] G. Pizzorusso, E. Fratini, J. Eiblmeier, R. Giorgi, D. Chelazzi, A. Chevalier, P. Baglioni, Physicochemical Characterization of Acrylamide/Bisacrylamide Hydrogels and Their Application for the Conservation of Easel Paintings, Langmuir 28 (2012) 3952–3961, https://doi.org/10.1021/la2044619.
[78] B. Hammouda, D.L. Ho, S. Kline, Insight into Clustering in Poly(ethylene oxide) Solutions, Macromolecules 37 (2004) 6932–6937, https://doi.org/10.1021/ma049623d.
[79] B. Hammouda, SANS from Polymers—Review of the Recent Literature, Polym. Rev. 50 (2010) 14–39, https://doi.org/10.1080/15583720903503460.
[80] M. Shibayama, Spatial inhomogeneity and dynamic fluctuations of polymer gels, Macromol. Chem. Phys. 199 (1998) 1–30, https://doi.org/10.1002/macp.1998.021990101.
[81] G.W. Scherer, Hydraulic radius and mesh size of gels, J. Sol-Gel Sci. Technol. 1 (1994) 285–291, https://doi.org/10.1007/BF00486171.
[82] L.M. Weber, C.G. Lopez, K.S. Anseth, Effects of PEG hydrogel crosslinking density on protein diffusion and encapsulated islet survival and function, J. Biomed. Mater. Res. Part A. 90A (2009) 720–729, https://doi.org/10.1002/jbm.a.32134.
[83] B. Hammouda, D.L. Ho, Insight into chain dimensions in PEO/water solutions, J. Polym. Sci. Part B Polym. Phys. 45 (2007) 2196–2200, https://doi.org/10.1002/polb.21221.
[84] C.M. Hansen, The Three Dimensional Solubility Parameter - Key to Paint Component Affinities I. - Solvents, Plasticizers, Polymers, and Resins, J. Paint Techn. 39 (1967) 104–117.
[85] C.M. Hansen, The Three Dimensional Solubility Parameter - Key to Paint Component Affinities II. - Dyes, Emulsifiers, Mutual Solubility and Compatibility, and Pigments, J. Paint Techn. 39 (1967) 505–510.
[86] C.M. Hansen, K. Skaarup, The Three Dimensional Solubility Parameter - Key to Paint Component Affinities III. - Independent Calculation of the Parameter Components, J. Paint Techn. 39 (1967) 511–514.
[87] L. Baij, J. Hermans, B. Ormsby, P. Noble, P. Iedema, K. Keune, A review of solvent action on oil paint, Herit. Sci. 8 (2020) 43, https://doi.org/10.1186/s40494-020-00388-x.
[88] L. Baij, J.J. Hermans, K. Keune, P.D. Iedema, Time-Dependent ATR-FTIR Spectroscopic Studies on Solvent Diffusion and Film Swelling in Oil Paint Model Systems, Macromolecules 51 (2018) 7134–7144, https://doi.org/10.1021/acs.macromol.8b00890.
[89] C.M. Hansen, Hansen Solubility Parameters A User's Handbook, Second Edition, CRC Press, Boca Raton, 2007.
[90] S. Abbott, H. Yamamoto, HSPiP Software, version 5.3.06, (2020).
[91] E. Carretti, L. Dei, R.G. Weiss, P. Baglioni, A new class of gels for the conservation of painted surfaces, J. Cult. Herit. 9 (2008) 386–393, https://doi.org/10.1016/j.culher.2007.10.009.
[92] T.L. Dawson, Examination, conservation and restoration of painted art, Color. Technol. 123 (2007) 281–292, https://doi.org/10.1111/j.1478-4408.2007.00096.x.
[93] C. Long, A. Li, H. Wu, Q. Zhang, Adsorption of naphthalene onto macroporous and hypercrosslinked polymeric adsorbent: Effect of pore structure of adsorbents on thermodynamic and kinetic properties, Colloids Surf. A Physicochem. Eng. Asp. 333 (2009) 150–155, https://doi.org/10.1016/j.colsurfa.2008.09.037.
[94] J.-H. Huang, K.-L. Huang, S.-Q. Liu, A.-T. Wang, C. Yan, Adsorption of Rhodamine B and methyl orange on a hypercrosslinked polymeric adsorbent in aqueous solution, Colloids Surf. A Physicochem. Eng. Asp. 330 (2008) 55–61, https://doi.org/10.1016/j.colsurfa.2008.07.050.
[95] X. Li, Y. Liu, D. Di, G. Wang, Y. Liu, A formaldehyde carbonyl groups-modified self-crosslinked polystyrene resin: Synthesis, adsorption and separation properties, Colloids Surf. A Physicochem. Eng. Asp. 500 (2016) 1–9, https://doi.org/10.1016/j.colsurfa.2016.03.061.